Does Stommel's Mixed Layer "Demon" Work?

RICHARD G. WILLIAMS,* MICHAEL A. SPALL,** AND JOHN C. MARSHALL*

*Center for Meteorology and Physical Oceanography, Department of Earth, Atmospheric, and Planetary Sciences, Massachusetts Institute of Technology, Cambridge, Massachusetts

**Department of Physical Oceanography, Woods Hole Oceanographic Institution,* Woods Hole, Massachusetts

(Manuscript received 20 June 1994, in final form 17 April 1995)

ABSTRACT

Stommel argued that the seasonal cycle leads to a bias in the coupling between the surface mixed layer and the main thermocline of the ocean. He suggested that a "demon" operated that effectively only allowed fluid at the end of winter to pass from the mixed layer into the main thermocline. In this study, Stommel's hypothesis is examined using diagnostics from a time-dependent coupled mixed layer–primitive equation model of the North Atlantic (CME). The influence of the seasonal cycle on the properties of the main thermocline is investigated using two methods. In the first, the rate and timing of subduction into the main thermocline is diagnosed using kinematic methods from the 1° resolution CME fields. In the second, tracer diagnostics of the CME and idealized experiments using a "date" tracer identifying the timing of subduction are performed. Over the subtropical gyre, both approaches generally support Stommel's hypothesis that fluid is only transferred from the mixed layer into the main thermocline over a short period, ~1 month, in late winter/early spring. Tracer date experiments are also conducted using the eddy-resolving 1/3° CME fields. Eddy stirring is found to enhance the rate at which the tracer spreads into unventilated regions, but does not alter the seasonal bias of the Stommel demon mechanism.

1. Introduction

Subduction is the process by which fluid transfers from the mixed layer into the thermocline. Iselin (1939) noted that the T–S properties in the main thermocline matched that of the winter mixed layer rather than that of its annual-mean state. Stommel (1979) explained this biased coupling by arguing that subduction into the main thermocline is an intermittent process, which only acts at the end of winter rather than continuously over the whole year. He suggested that a "demon" effectively operated,[1] selecting the properties of the mixed layer that pass into the underlying thermocline. This selective transfer occurs whenever fluid parcels subducted from the mixed layer are advected only a short distance compared with the seasonal migration of density outcrops (Fig. 1).

Stommel's hypothesis appears to be supported by the short subduction period diagnosed from climatological observations over the North Atlantic by Marshall et al. (1993, henceforth referred to as MNW); however, these diagnostics could be questioned due to uncertainties in the observations. Stommel's idea is assumed in steady thermocline models that employ end of winter boundary conditions. In contrast, climate models often apply annual-mean boundary conditions, which may misrepresent the coupling between the surface and deep ocean. Luyten et al. (1983, henceforth LPS) first examined ventilation using a thermocline model with imposed density outcrops chosen from end of winter variations. This has been followed by thermocline models incorporating end of winter variations in both the thickness and density of the mixed layer (Williams 1989, 1991; Huang 1990; Marshall and Nurser 1991; Pedlosky and Robbins 1991). The subduction process has also been explicitly resolved and examined using a coupled mixed layer–isopycnal model by Bleck et al. (1989) and New et al. (1995), and with time-dependent idealized thermocline models by Liu and Pedlosky (1994) and Marshall and Marshall (1995).

In this study, we wish to focus on Stommel's hypothesis using diagnostics from the U.S. Community

* Woods Hole Oceanographic Institution Contribution Number 8405.

[1] Stommel made an analogy with the "demons" introduced by James Clerk Maxwell in his studies of the kinematic theory of gases. The demons were placed in charge of trap doors in a partition dividing a gas into two chambers. The demons were clever enough to estimate the velocities of molecules and agile enough to open and close the trap doors in time to allow or prevent the passage of any particular molecule through the door, and so allow the fast molecules to accumulate on one side of the partition.

Corresponding author address: Dr. Richard G. Williams, Oceanography Laboratories, Dept. of Earth Sciences, University of Liverpool, Bedforth Street North, P.O. Box 147, Liverpool L69 3BX, United Kingdom.
E-mail: ric@liverpool.ac.uk

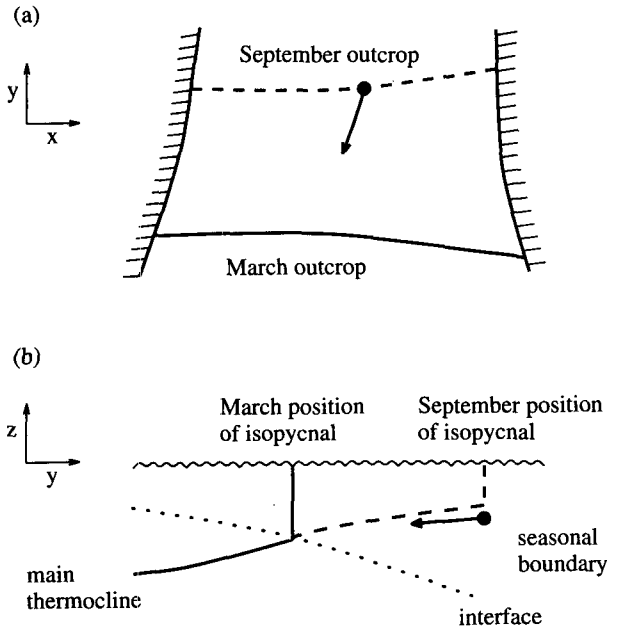

FIG. 1. A schematic diagram illustrating the Stommel demon mechanism in (a) a plan view at the sea surface and (b) a meridional section. Over the cooling season in the Northern Hemisphere the outcrop of a density surface migrates equatorward from September to March (denoted by dashed and full lines). Consider a fluid parcel (circle) subducted from the vertically homogeneous mixed layer and advected equatorward along this density surface. If the fluid parcel is advected past the March outcrop during the year, then it is subducted in to the main thermocline [the upper extent of which is shown by the dotted line in (b)].

Model (CME) of the North Atlantic. The study concentrates on the subduction associated with the large-scale circulation of the gyre sweeping fluid to and from a time-dependent mixed layer into the thermocline. It extends previous analytical models based on the thermocline equations by including the seasonal cycling of the mixed layer and higher-order primitive equation balances. In the present study, we focus our attention on the 1° resolution CME calculation (briefly described in section 2) but also present tracer results using model fields from the 1/3° CME integration. The latter results are important as it has been argued that eddy processes could play a role in ventilating the main thermocline across frontal regions (see, e.g., Pollard and Reiger 1992).[2]

The impact of the seasonal cycle on the properties of the main thermocline is diagnosed using two independent methods applied to the model fields from the CME. In the first, the rate and period over which fluid is transferred from the mixed layer into the main thermocline are found kinematically from the mixed layer cycle and velocity fields from the CME (section 3). In the second, the ventilation of tracers is examined by conducting experiments with an idealized "date" tracer that highlights the exact timing of subduction, as well as by diagnosing the traditional T–S properties and "age" tracer from the CME fields (section 4). Finally, the role of eddy stirring is examined by repeating the date tracer experiments using the 1/3° CME fields (section 5).

2. The CME Model

The subduction process is investigated using diagnostics from the U.S. Community Model of the North Atlantic integrated by Bryan and Holland (1989). The CME is based on the finite-difference form of the primitive equations presented by Bryan (1969) and documented by Cox (1984), which is extended by Bryan and Holland (1989) to include an embedded surface mixed layer model and an implicit diffusive parameterization of the vertical convection process. The turbulent mixing within the surface boundary layer is parameterized in a similar manner to the bulk kinetic energy model of Camp and Elsberry (1978). The energy available for deepening of the mixed layer from the surface forcing is converted into potential energy and distributed over the depth of the mixed layer. Detrainment of the mixed layer is included such that if the mixed layer shallows the deeper remnants of the old mixed layer remain.

The model domain extends from 15°S to 65°N in the North Atlantic basin with 30 levels in the vertical. The horizontal resolution is 1° in latitude and 1.2° in longitude in the noneddy resolving version. The model was initialized with Levitus (1982) winter conditions and integrated for 45 years with surface wind stress and buoyancy forcing. The surface stress is from the monthly mean climatology of Hellerman and Rosenstein (1983). The surface heat flux is derived by relaxing the surface temperature of the model to the apparent atmospheric temperature with a restoring timescale of typically 50 days, which varies with position, time of year, and sea surface temperature. The net freshwater flux at the surface is parameterized by relaxing the surface salinity toward the monthly mean climatology of Levitus (1982) with a timescale of 50 days. The model fields from the last year of the 45-year integration are used in the following subduction diagnostics.

The transport streamfunction of the model, Fig. 2, shows anticyclonic and cyclonic circulations in the subtropical and subpolar gyres with an intense western boundary current. The horizontal velocities are typically 1 cm s^{-1} in the interior of the subtropical gyre with the transport concentrated in the upper 1 km. In the 1° version of the model, geostrophic eddies are not

[2] Eddy processes probably drive intense subduction locally along a front. However, scaling arguments by Follows and Marshall (1994) and modeling studies by Spall (1995) suggest that this frontal subduction when globally averaged over a basin is smaller than the subduction rates of ~100 m/yr from the mean circulation deduced from climatological data by MNW.

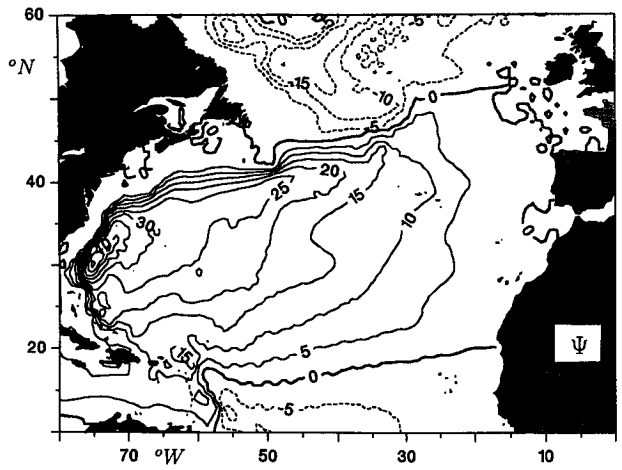

FIG. 2. Annual-mean transport streamfunction for the CME model (10^6 m^3 s^{-1}).

resolved, and the western recirculation appears relatively weak.

The mixed layer depth, h, and σ_θ fields at the spring equinox, Fig. 3, generally become deeper and denser with latitude due to the increasing annual surface buoyancy loss; h is defined by the depth at which σ_θ differs by 0.05 from the surface σ_θ. There is a striking front in mixed layer depth[3] crossing the subtropical gyre, though the front is not apparent in the surface density and velocity fields. The sharp change in mixed layer depth strongly influences the local subduction rate and appears to be correlated with the underlying large-scale potential vorticity Q (Fig. 4); however, it does not appear to significantly affect the seasonal coupling between the surface and deep ocean (see results in sections 3c and 4c). In reality, density fronts associated with mesoscale processes are probably more significant than these mixed layer depth fronts. Nonetheless, the sharp changes in mixed layer depth revealed in Fig. 3 are probably more realistic than the smooth climatology compiled in Levitus (1982).

3. Subduction rate and period

a. Lagrangian view

The subduction process is illustrated here by following a parcel as it is swept around a subtropical gyre, echoing previous studies with idealized mixed layer models (e.g., Federiuk and Price 1985; Woods 1985; Cushman-Roisin 1987). The parcel trajectory is found by inverting the kinematic relation

$$\frac{d\mathbf{x}}{dt} = \mathbf{u}(\mathbf{x}, t), \tag{1}$$

using 3-day velocity fields of the CME with a fourth-order Runge–Kutta scheme; here, $\mathbf{x}$ represents the position of the parcel at time t, and $\mathbf{u}$ is the three-dimensional velocity vector. When the parcel passes through the mixed layer, vertical mixing is assumed to reset the properties associated with the parcel, rather than change the vertical position of the parcel.

The parcel is released in the summer (year 0.5) at a depth of 50 m and at 40°N, 30°W in the subtropical gyre and tracked for the subsequent 7.5 years (Fig. 3a). The parcel glides downward under the influence of Ekman pumping while being swept around the gyre (Fig. 5a). The overlying mixed layer exhibits a seasonal cycle due to the seasonal buoyancy forcing with an over-

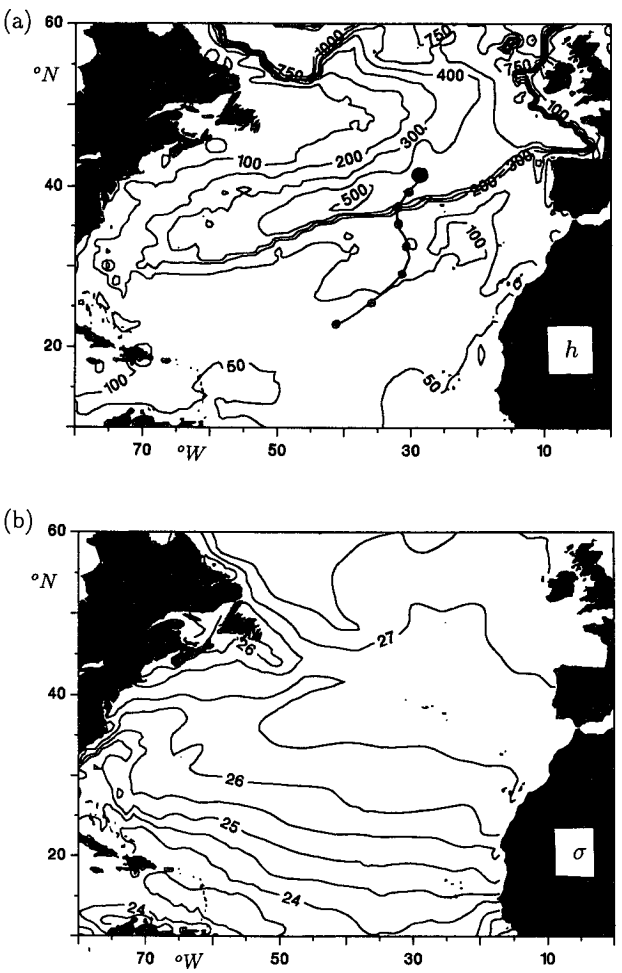

FIG. 3. (a) Mixed layer depth (m) and (b) density close to the spring equinox (day 79). The path of a Lagrangian parcel introduced at 40°N, 30°W at year 0.5 and followed for 7.5 years is shown with circles indicating the position on the trajectory at the start of each year.

[3] Similar mixed layer depth fronts are found in other models that do not resolve the Rossby deformation radius, such as in the 1° isopycnal model (New et al. 1995).

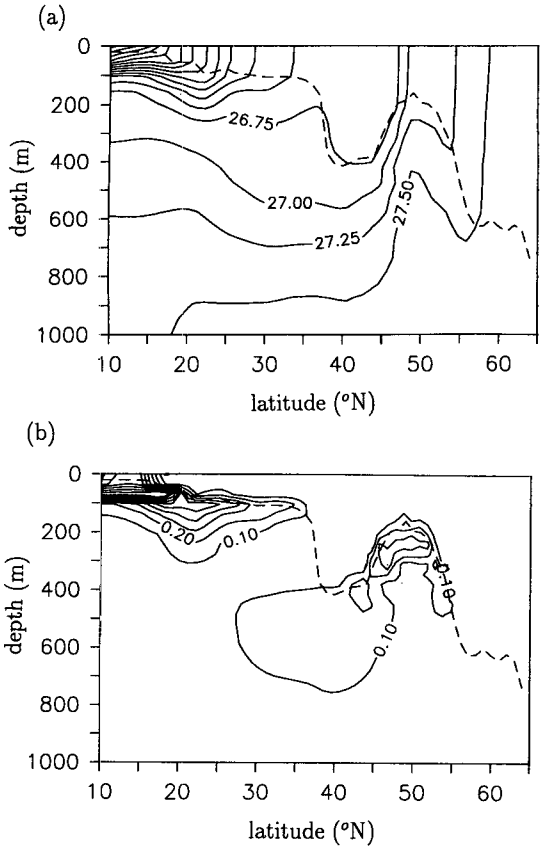

FIG. 4. North–south section along 30°W close to the spring equinox (day 079) showing the mixed layer depth (dashed line) with (a) potential density and (b) the large-scale potential vorticity (10^{-9} m^{-1} s^{-1}).

all warming and shallowing as the parcel is swept south.

During the first three years, the parcel is repeatedly subducted into the seasonal thermocline and reentrained by the mixed layer in the following winter. While in the thermocline, the parcel is cooler than the overlying mixed layer and has a larger stratification and associated potential vorticity (Figs. 5b,c). The mixed layer shows a larger temperature cycle due to the surface forcing, although the subducted parcel continues to warm in summer and autumn through the vertical diffusion of heat. When the parcel is reentrained, temperature and stratification are reset to the values of the mixed layer.

The parcel finally enters the main thermocline in mid-April of the fourth year (year 3.4 at 35°N, 34°W) and avoids being reentrained by the mixed layer in the following winter. The temperature and potential vorticity of the parcel are subsequently nearly conserved and decoupled from the seasonal cycle of the overlying mixed layer.

In this fourth year of the trajectory, subduction from the mixed layer leads to an annual volume flux per unit horizontal area of 60 m/yr into the main thermocline. The volume flux is comprised of 20 m/yr from the vertical transfer and 40 m/yr from lateral transfer through the shoaling mixed layer. Following this parcel, subduction into the main thermocline only occurs over a short period of 27 days extending from the end of winter in mid-March until mid-April. Any parcels subducted after this period enter the seasonal thermocline and are re-entrained into the mixed layer in the following winter.

In summary, the Lagrangian study appears to generally support Stommel's hypothesis that the mixed layer and main thermocline are only coupled in late winter. In the following section, we diagnose the subduction rate and period over the modeled North Atlantic.

b. Subduction rate

The instantaneous subduction rate, $S(t)$, or volume flux of mixed layer fluid entering the thermocline (relative to the base of the instantaneous mixed layer) per unit horizontal area (Cushman-Roisin 1987) is defined by

$$S(t) = -w_b - \frac{Dh}{Dt_b}. \tag{2}$$

The first term represents the vertical transfer of fluid, and the second term the temporal and lateral transfer in the Lagrangian frame; here, $D/Dt_b = \partial/\partial t + \mathbf{u}_b \cdot \nabla$, and w_b and $\mathbf{u}_b$ are the vertical and horizontal velocities at the base of the mixed layer.

In a Lagrangian frame, the annual flux into the main thermocline, S_{ann}, can be defined as the instantaneous subduction rate integrated over 1 year ($\mathcal{T}_{\text{year}}$) from the end of the first winter W_1 to the second winter W_2:

$$S_{\text{ann}} = \frac{1}{\mathcal{T}_{\text{year}}} \int_{W_1}^{W_2} S(t)\,dt$$

$$= -\frac{1}{\mathcal{T}_{\text{year}}} \left(\int_{W_1}^{W_2} w_b\,dt + h(W_2) - h(W_1) \right). \tag{3}$$

The Lagrangian frame is chosen to track parcels swept around the gyre at the base of the instantaneous mixed layer; following a different depth within the seasonal thermocline changes the appropriate definition for S_{ann}, but only alters the detail of the results. As shown in Fig. 6, the annual subduction in the Lagrangian frame depends on the integrated vertical transfer and the shoaling of the mixed layer between the end of winters W_1 and W_2.

Here S_{ann} is inferred from the Lagrangian definition using the velocity and mixed layer cycle in the CME as revealed by 9-day dumps of the model fields. At every grid point in the basin, the trajectory of a fluid column is determined, which follows the flow at the base of the instantaneous mixed layer. The trajectory

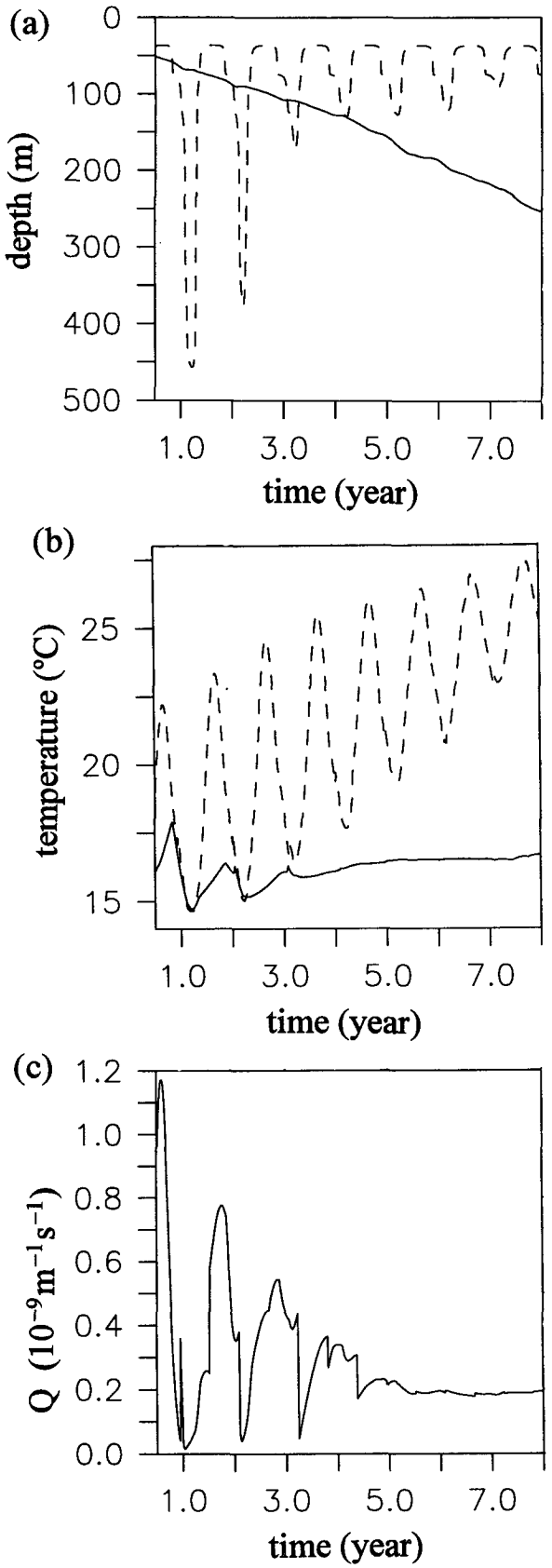

starts at the end of the first winter W_1 and finishes at the second winter W_2 (the end of winter is defined by a local maximum in the mixed layer density). Then S_{ann} is evaluated along the trajectory using (3) by summing the vertical transfer and the lateral transfer between the start and end points W_1 and W_2.

The derived subduction rate, S_{ann}, is shown in Fig. 7a with values plotted at the starting grid point of the trajectory. We wish to focus on the broad patterns of S_{ann}, rather than detailed variations which are noisy and possibly unrealistic (due to the combination of the Lagrangian method and model fields). In the subtropical gyre, S_{ann} is typically 50 m/yr, increasing to over 200 m/yr across the mixed layer front. The vertical transfer of fluid makes the largest contribution to the subduction rate over most of the subtropical gyre (Fig. 7b). However, the lateral transfer of fluid dominates in the vicinity of the front where the anticyclonic circulation sweeps fluid from the shoaling mixed layer into the stratified thermocline. The subduction signal of the front extends laterally the distance a particle moves in 1 year, typically 500 km; using an Eulerian definition for S_{ann} of the volume flux through the base of the winter mixed layer (as in MNW) leads to the subduction signal, which is even more concentrated along the few grid points resolving the front.

In the subpolar gyre, there is widespread entrainment with fluid swept from the main thermocline into the seasonal boundary layer; S_{ann} is typically -100 m/yr to -300 m/yr. However, in the northwest corner of the gyre, there is substantial subduction (although noisy) due to the cyclonic circulation sweeping fluid from the shoaling mixed layer into the thermocline.

In comparison, the climatological estimates of MNW show widespread subduction in the subtropical gyre, S_{ann}, typically 50–100 m/yr, and conversely entrainment over the subpolar gyre, S_{ann}, typically -100 and -300 m/yr (see their Fig. 5). These modeled subduction rates differ from the climatological estimates by showing the frontal signal in the subtropical gyre and, possibly more realistically, by showing subduction in the northwest corner of the subpolar gyre.

c. *Subduction period*

The subduction period is defined by the time over which fluid is irreversibly transferred from the mixed layer into the main thermocline. In a Lagrangian frame, the annual subduction into the main thermocline is equivalent to the instantaneous subduction integrated

FIG. 5. Properties of a parcel following the trajectory shown in Fig. 3a from 0.5 to 8 years: (a) depth of parcel (solid line) and overlying mixed layer (dashed line), (b) temperature of parcel (solid line) and overlying mixed layer (dashed line), and (c) large-scale potential vorticity of the parcel (10^{-9} m^{-1} s^{-1}).

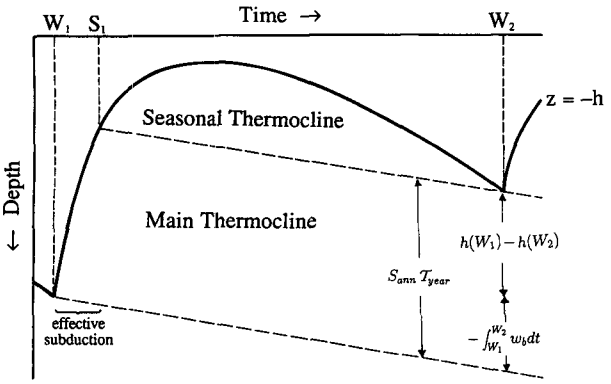

FIG. 6. A schematic mixed layer cycle following a water column in a Lagrangian frame over 1 year; the mixed layer depth and subducted isopycnals are indicated by full and dashed lines. The annual subduction S_{ann} into the main thermocline depends on the integrated vertical transfer and the shoaling of the mixed layer between the end of winter W_1 and W_2. Fluid enters the main thermocline during a subduction period extending from the end of winter W_1 until a later time S_1.

over the effective period W_1 to S_1 (as shown in Fig. 6 and discussed in MNW):

$$S_{\text{ann}} = \frac{1}{\mathcal{T}_{\text{year}}} \int_{W_1}^{S_1} S(t)dt. \qquad (4)$$

The effective subduction period is diagnosed in (4) using the previous estimate of S_{ann} and our knowledge of the velocity and mixed layer depth cycle from the CME fields. In the limit of no subduction, the subduction period is zero ($S_1 = W_1$), whereas in the limit of no seasonal mixed layer cycle, the subduction period extends to 1 year ($S_1 = W_2$).

The subduction period found in the model is short—only 1 mo—over most of the subtropical gyre (Fig. 8). In the vicinity of the front, where there is extensive subduction, the period remains short because of the rapid mixed layer shallowing following particles as they traverse the front. The period lengthens to 2 or 3 mo in the Tropics because of the less pronounced cycle in the mixed layer depth. In the subpolar gyre, the subduction period reflects the time period over which fluid is irreversibly entrained into the mixed layer. The entrainment period is typically 2–4 mo over the subpolar gyre (indicated by negative values in Fig. 8).

The derived subduction period is in excellent agreement with the climatological study of MNW (see their Fig. 6). They diagnose the period from a kinematic estimate of S_{ann} and by making use of $S(t)$ derived from the buoyancy forcing. They find that the subduction period is typically 1 mo over the subtropical gyre and lengthens to 3 mo in the Tropics.

In summary, our kinematic diagnostics show a short subduction period, which suggests that fluid is only transferred from the mixed layer into the main thermocline over a short period after the end of winter—supporting Stommel's "demon" hypothesis.

4. Tracer fields

We now examine how subduction influences the tracer distribution within the main thermocline.

a. Water mass properties

The tracers most readily available in the ocean are the temperature–salinity (T–S) properties. Iselin (1939) first noted the similarity between the T–S variation with depth in the subtropical gyre and that of the winter mixed layer at high latitudes. We now examine whether there is a similar correspondence in the T–S variation within the CME model. The modeled T–S profile in the main thermocline at 30°N, 30°W is shown as the full line in Fig. 9, which closely agrees with that

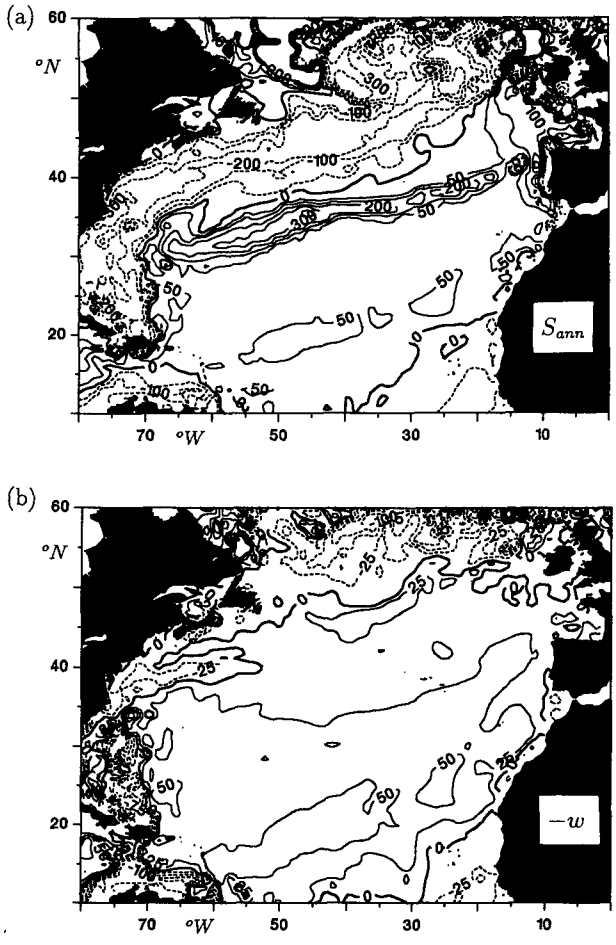

FIG. 7. Kinematic calculation for (a) annual subduction rate S_{ann} (m/yr) into the main thermocline, (b) annual vertical flux into the main thermocline; positive values indicate subduction into the main thermocline, whereas negative values indicate entrainment into the seasonal boundary layer.

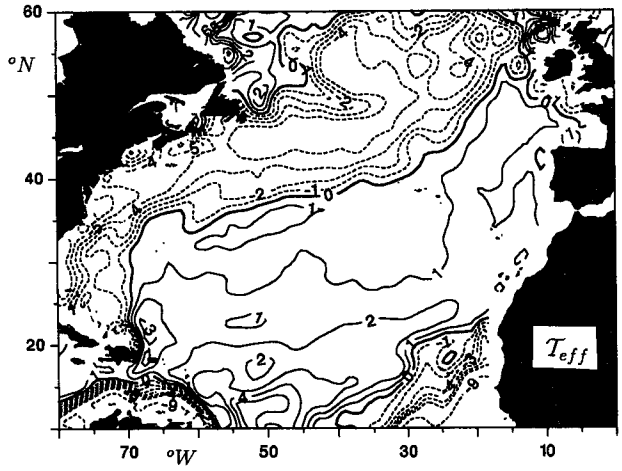

FIG. 8. Subduction period in months inferred from the kinematic estimate of the subduction rate and the seasonal mixed layer cycle; positive values indicate a subduction period extending from the end of winter, whereas negative values indicate an entrainment period prior to the end of winter.

from the Levitus winter climatology (dashed line in Fig. 9). The corresponding upstream T–S values in the summer and winter mixed layer are shown as squares and circles in Fig. 9. These upstream values are found from where trajectories at 30°N, 30°W (over a depth range of 90–370 m) thread back and intersect the summer or winter mixed layer. The T–S of the mixed layer in summer is much warmer and saltier than the T–S curve found in the main thermocline, as shown by the displacement between the squares and full line in Fig. 9. In contrast, the T–S of the mixed layer in winter is very close to that of the main thermocline over the temperature range of the North Atlantic Central Waters (14.5°–18.5°C).

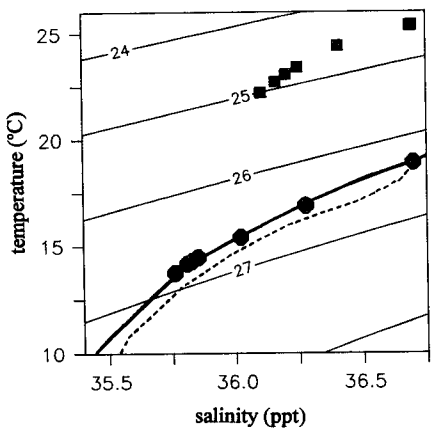

FIG. 9. A T–S curve within the main thermocline at 30°N, 30°W with the solid line from the 1° degree model and dashed line from the Levitus (1982) annual-mean climatology. The T–S properties at the outcrop location in winter (circles) and summer (squares) are shown for parcels now within the thermocline at 30°N, 30°W.

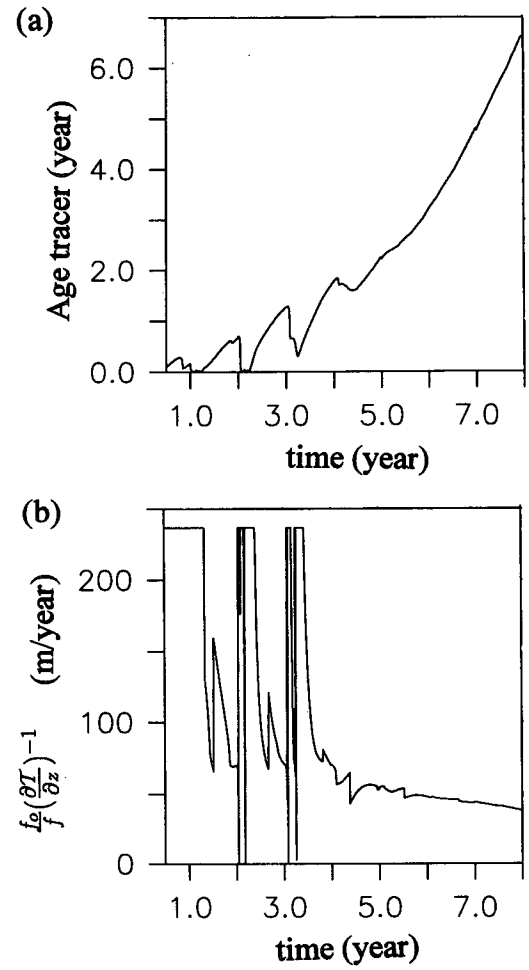

FIG. 10. (a) Age tracer (years) of the parcel following the trajectory shown in Fig. 3a from 0.5 to 8 years. (b) Subduction rate (m/yr) derived from the vertical gradients in the age tracer for the same parcel.

Fluid colder than 14.5°C is not subducted within the subtropical gyre and lies within the unventilated pool. The interface between the ventilated and unventilated regions is marked by a change in slope of the T–S curve, which has also been seen in hydrographic observations from the eastern North Atlantic (M. McCartney 1993, personal communication).

b. Age tracer

An age tracer $\mathcal{T}$ is carried in the CME integration and effectively measures the elapsed time since fluid was in the mixed layer. The age is set to zero at the surface of the model, and is found elsewhere in the CME model by solving an advection and diffusion equation.

The seasonal cycle of the age is shown in Fig. 10a for the Lagrangian float discussed in section 2. During

the first three years, the float repeatedly passes from the mixed layer to the seasonal thermocline with the age reset in the mixed layer and increasing with time in the thermocline. Eventually, when the parcel is finally subducted into the main thermocline, the age continues to increase and roughly measures the elapsed time since subduction. However, the age tracer does increase at a slightly faster rate than 1 yr/year due to an enhancement by diffusion from poorly ventilated regions where fluid is old.

The subduction rate implied by the age field is shown in Fig. 10b using the diagnostic relationship by Jenkins (1987):

$$S_{\mathcal{T}} = \frac{f_0}{f}\left(\frac{\partial \mathcal{T}}{\partial z}\right)^{-1}. \qquad (5)$$

This elegant relation connects the upstream subduction rate with the vertical gradient in the age field, $\partial\mathcal{T}/\partial z$, observed downstream modulated by the change in the planetary vorticity at the outcrop, f_0, and at the site of the observations, f; a derivation of this relation, which did not appear obvious to us, is given in appendix A. The subduction estimate based on (5) is noisy until the float is well within the main thermocline with $S_{\mathcal{T}} \sim 50$ m/yr in year 4 and slightly decreasing to 40 m/yr by year 8. This estimate is reasonably close to the previous kinematic estimate of 60 m/yr; in other cases, there is similar agreement of within 30%, but it can be larger or smaller than the kinematic estimate. These differences may be due to the difficulty in inferring $S_{\mathcal{T}}$ due to the rotation of the velocity field with depth and diffusion of the age field.

The age distribution along the $\sigma_\theta = 26.5$ surface in March is shown in Fig. 11. The age field appears consistent with the ventilated picture of the gyre; fluid is subducted in the northeast Atlantic and increasing in age as it is swept around the subtropical gyre. On this σ_θ surface, ventilated fluid takes typically 10 years to pass from the outcrop to the western boundary. Unventilated regions in the western pool and Tropics are clearly marked by their relatively large age, 10–15 years, which is probably set by the diffusion of younger age from the surrounding ventilated regions (the maximum age in the model integration is 45 years). The overall pattern of the age distribution is broadly in accord with that inferred from tritium–helium observations by Jenkins (1988), although the modeled values are older than those observed on the $\sigma_\theta = 26.5$ surface and are closer to those on the $\sigma_\theta = 26.75$ surface. The observations though do not clearly show the unventilated western pool, perhaps due to insufficient resolution there or because it is masked by vigorous eddy stirring (see section 5).

Ventilated fluid appears to have a relatively smooth age distribution near the outcrop of the σ_θ surface. The age field does not show any fronts marking a transition of subducted fluid from one winter to the next (Fig. 11), whereas they are seen in a mixed layer model study by Federiuk and Price (1985). Thus, the age distribution does not appear to show a signal supporting Stommel's hypothesis that fluid is only subducted at the end of winter. The lack of these age fronts in both the CME and the age observations of Jenkins (1987) in the beta-triangle site is probably due to the relatively coarse resolution and diffusive spreading of any age fronts, rather than implying that subduction acts over the entire year. This issue is explored further in the following idealized tracer experiment.

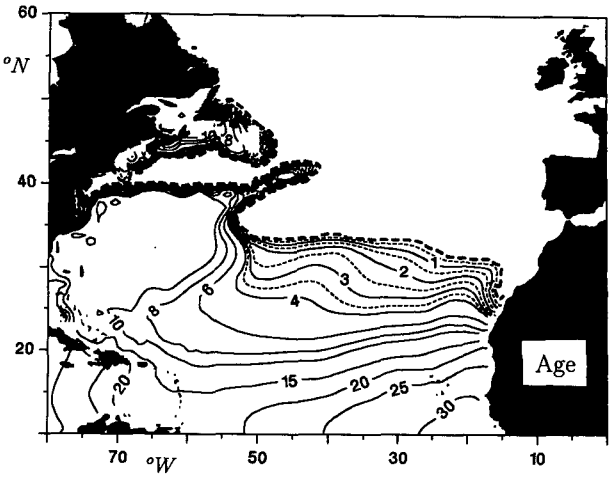

FIG. 11. Age tracer (years) on the $\sigma_\theta = 26.5$ surface in March; the outcrop is indicated by the thick dashed line and 1/2 year marks by the short dashed lines.

c. Date tracer

We now examine ventilation using an idealized "date" tracer, A, that identifies the timing of subduction. We can imagine the tracer represents a rainbow of colored dyes injected into the mixed layer, which have a value set *every* year to 0 at the start of January and increasing linearly to 1 by the end of December. The tracer field in the underlying interior is initially set to an unphysical value of -0.05 and subsequently evolves as it is advected and diffused from the source in the mixed layer:

$$\frac{\partial A}{\partial t} = -\nabla\cdot(\mathbf{u}A) + \nabla(k\nabla A). \qquad (6)$$

The tracer equation is integrated for 10 years using velocity fields taken every 3 days from the final year of the 1° CME integration; the integration uses an Euler-forward scheme with "upwind" differencing, a small explicit horizontal diffusion of 10 m^2s^{-1}, and no vertical diffusion (further details are given in appendix B).

The tracer field on the $\sigma_\theta = 25$, 26.5, and 27 surfaces in September of year 9 and the following March of year 10 are shown in Fig. 12. In the figure, the tracer values

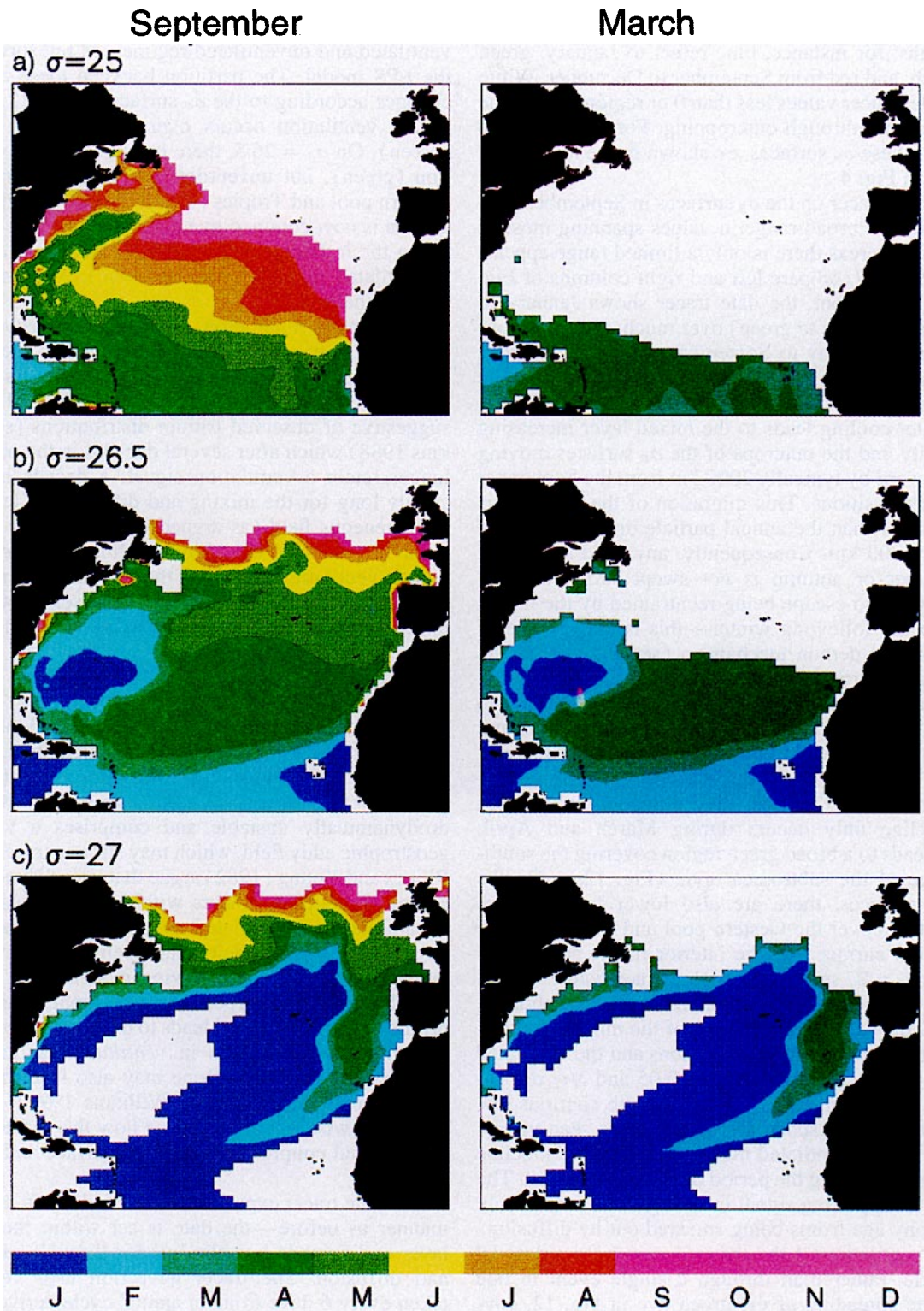

FIG. 12. Date tracer for the 1° degree model along (a) $\sigma_\theta = 25$ surface in September of year 9 and March of year 10, (b) $\sigma_\theta = 26.5$ surface in September of year 9 and March of year 10, and (c) $\sigma_\theta = 27$ surface in September of year 9 and March of year 10. The date tracer is colored and identifies the time of year fluid is subducted from the mixed layer into the underlying thermocline; white indicates regions of no tracer in poorly ventilated regions or where the σ_θ surface outcrops to the north.

over the physical range 0–1 are colored to correspond to months; for instance, blue refers to January, green to March, and red from September to December. White delineates tracer values less than 0 or regions where the σ_θ disappears through outcropping. For reference, the depth of these σ_θ surfaces are shown in the meridional section in Fig. 4.

The date tracer on the σ_θ surfaces in September generally show a broad range in values spanning most of the year, whereas there is only a limited range appearing in March (compare left and right columns of Fig. 12). In September, the date tracer shows January to April values (blue to green) over much of the subtropical gyre with May to September values (light green through to red) at higher latitudes close to where the σ_θ surface outcrops in summer and autumn. However, the winter cooling leads to the mixed layer increasing in density and the outcrops of the σ_θ surfaces moving equatorward by typically 2000 km from the September to March positions. This migration of the outcrops is much larger than the annual particle displacements of typically 300 km. Consequently, any fluid subducted in summer or autumn is not swept sufficiently far downstream to escape being reentrained by the mixed layer in the following winter—this is the essence of the Stommel demon mechanism (see Fig. 1). In the following March, the tracer shows a much reduced range only extending from January to April (blue to green in Fig. 12). Thus, the mixed layer in summer and autumn is not directly coupled with the main thermocline.

On the $\sigma_\theta = 25$ surface, the ventilation into the main thermocline only occurs during March and April, which leads to a broad green region covering the southern edge of the subtropical gyre (Fig. 12a). On the deeper surfaces, there are also lower tracer values (blue) that cover the western pool and Tropics on the $\sigma_\theta = 26.5$ surface and the interior of the subtropical gyre on $\sigma_\theta = 27$ surface. These low tracer values (blue) are not due to direct ventilation in January or February. Instead, they are a consequence of the mixing and diffusion between the initial conditions and the ventilated waters (with typical values of -0.05 and $3/12$ respectively). These unventilated regions with spurious low dates (blue) correspond to the high ages seen in Fig. 11. Therefore, ventilated fluid in the main thermocline is subducted during the period of March and April. The lack of a supporting signal in the age field is probably due to any age fronts being smeared out by diffusion.

The ventilation of the tracer occurs over a decadal timescale, rather than through a single event in one year; the spreading of the green dye in Fig. 12, covering much of the subtropical gyre, is the result of 10 years of ventilation. Temporal variability in the main thermocline may result from interannual changes in these end of winter boundary conditions, even though much of the seasonal cycle is decoupled from the main thermocline.

The patterns of the date tracer highlight the different ventilated and unventilated regimes, as put forward in the LPS model. The partition between these regimes changes according to the σ_θ surface in Fig. 12. On $\sigma_\theta = 25$, ventilation occurs over most of the surface (green). On $\sigma_\theta = 26.5$, there is still extensive ventilation (green), but unventilated regions appear in the western pool and Tropics (blue). On $\sigma_\theta = 27$, the ventilation is now confined to a narrow plume (green) entering the interior along the eastern boundary and the unventilated region (white and blue) expands to fill most of the gyre.

In the tracer integration, the distinction between the ventilated and unventilated regimes must eventually disappear as the whole of the σ_θ surface takes up the boundary values of March and April. This final state is suggestive of observed tritium distributions (see Jenkins 1988) which after several decades in the ocean no longer retain a ventilation signal; a decade is sufficiently long for the mixing and diffusion to lead to a homogeneous field (as argued by Rhines and Young 1982). In contrast, the tritium–helium age *does* show a clear ventilation signal, as the helium concentration is reset to nearly zero whenever it passes through the mixed layer through outgassing to the atmosphere.

5. Role of eddy stirring

Tracer date experiments were also carried out using velocity fields from the $1/3°$ CME calculation, which had been integrated for 25 years by Bryan and Holland (1989). At this resolution, the large-scale flow is hydrodynamically unstable and comprises a vigorous geostrophic eddy field, which may stir any tracer fields. Rhines and Young (1982) argue that lateral fluxes from eddies homogenize tracers within closed geostrophic streamlines in unventilated regions. This homogenization of potential vorticity has been demonstrated in quasigeostrophic eddy-resolving models. Cox (1985) also showed that incorporating geostrophic eddies in a primitive equation model leads to the potential vorticity becoming more uniform in *ventilated* regions; note though that ventilation alone may also lead to nearly uniform potential vorticity (Williams 1991). In this study, we wish now to examine how the eddies affect the seasonal coupling between the surface and the interior.

The date tracer experiment is carried out in the same manner as before—the date is set within the mixed layer and spreads into the interior through advection and diffusion. The tracer advection uses velocities taken every 6 days from an annual cycle derived from the last 5 years of the $1/3°$ CME integration. The tracer model is integrated for 10 years with the resulting date fields for $\sigma_\theta = 25$, 26.5, and 27 surfaces in September of year 9 and March of year 10 shown in Fig. 13; this should be compared with the coarse-resolution results in Fig. 12.

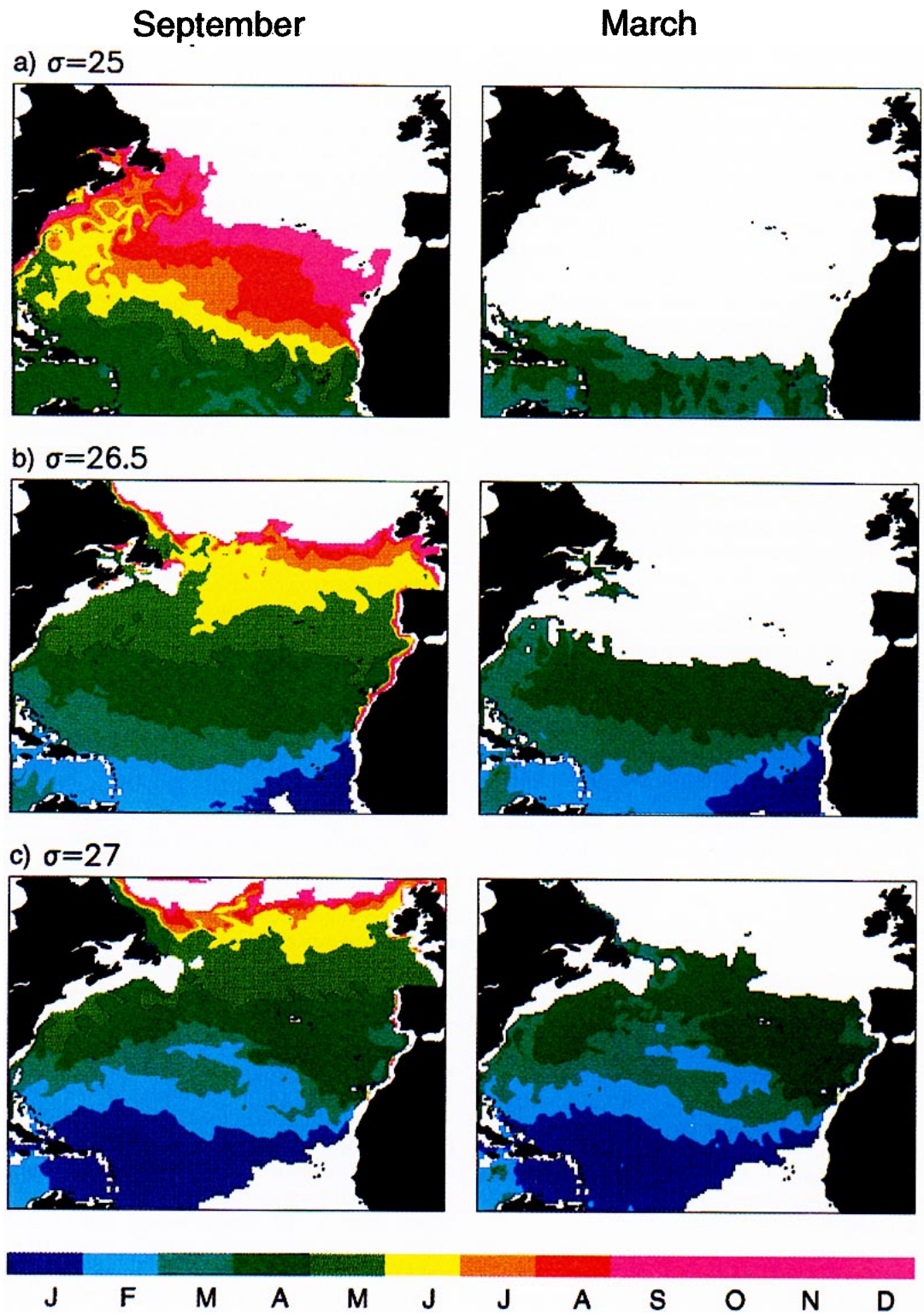

FIG. 13. Date tracer for the $1/3°$ degree model along (a) $\sigma_\theta = 25$ surface in September of year 9 and March of year 10, (b) $\sigma_\theta = 26.5$ surface in September of year 9 and March of year 10, and (c) $\sigma_\theta = 27$ surface in September of year 9 and March of year 10. The color scheme is the same as in Fig. 12.

In September, there is again a broad range in the values of the date tracer spanning the seasonal cycle. The eddy stirring can be vividly seen in Fig. 13a around the Gulf Stream through the striking "wind up" of the tracer field. If this eddy stirring is the dominant ventilation mechanism, then one might expect to see fluid from all seasons passing into the main thermocline—there would either be a rainbow of colors entering the thermocline or a smearing of the colors into the annual mean. However, as in the 1° degree model, the seasonal migration of the outcrops is so large that only March and April fluid (green) succeed in passing into the main thermocline; see the extensive green dye spreading across the thermocline in March in Fig. 13. Therefore, the seasonal bias in the coupling between the surface and the interior remains the same, even in the presence of strong eddy stirring.

The most striking effect of the eddies is the enhanced tracer transfer into regions that were previously poorly ventilated, such as the western pool, the shadow zone along the southern edge of the subtropical gyre, and the Tropics. Incorporating the eddies has increased the extent of the March/April fluid (green) on the denser surfaces probably through a shear–dispersal mechanism, where the tracer is diffused across mean streamlines by eddies and then advected by the mean flow throughout the gyre. The eddy diffusivity is crudely estimated here from $k \sim L^2/(\pi t)$, which gives $k \sim O(1000\ \mathrm{m^2\ s^{-1}})$, assuming that $L \sim 1000$ km measures the distance the tracer spreads across streamlines and $t \sim 10$ years is the timescale of spreading. After a decade, the pattern of the tracer field does not now highlight the different dynamical regimes and makes it difficult to identify where ventilation or eddy stirring is the dominant process.

6. Conclusions

The seasonal coupling of the mixed layer and the main thermocline has been studied with kinematic and tracer diagnostics from a coupled mixed layer–primitive equation model of the North Atlantic (CME). The mixed layer cycle appears to act as a "trap door," allowing only the late winter properties of the mixed layer through into the main thermocline. Stommel drew an analogy with the trap door operated by the demons introduced by Maxwell in his investigation of the kinematic theory of gases. This process is certainly at work within the CME.

Kinematic diagnostics of the subduction rates and periods from the 1° CME model broadly resemble those patterns deduced by MNW using climatological hydrographic and surface fluxes. The subduction rate is enhanced over the Ekman pumping in the subtropical gyre by the lateral induction of fluid through the shoaling mixed layer. The subduction period is generally short, lasting 1 month after the end of winter over the subtropical gyre, and becoming somewhat longer toward the Tropics where the seasonal mixed layer cycle is less pronounced.

The Stommel demon mechanism is illustrated using an idealized tracer experiment in which a rainbow of colored dyes are added to the mixed layer and allowed to advect or diffuse into the interior. The experiment reveals that only tracers originating from the mixed layer in March or April pass into the main thermocline, which is due to the seasonal migration of the outcrops being so much larger than the annual displacement of fluid parcels. Any other tracer subducted during summer or autumn into the seasonal thermocline is reentrained during the winter cooling and deepening of the mixed layer. This biased coupling is supported by diagnostics of the T–S relation in the CME that show the properties of the main thermocline matching those of the winter mixed layer. While the experiments suggest that much of the seasonal variability in the mixed layer is decoupled from the main thermocline, interannual changes in the end of winter conditions may lead to temporal variability penetrating into the main thermocline.

The subduction process may be modified by the presence of geostrophic eddies and fronts, which may *locally* enhance the subduction rate and perhaps lengthens the subduction period. However, the date tracer experiments using velocity fields from the $1/3°$ degree CME model show that, in an integral sense, gross aspects of the subduction process are unaffected. The geostrophic eddies assist in the lateral spreading of the tracer but do not alter the seasonal coupling with the surface.

The transfer of gases between the atmosphere and the main thermocline will be influenced by the interplay between the Stommel demon mechanism and the air–sea equilibration timescale for the gas. The equilibration timescale of oxygen, carbon dioxide, and radiocarbon for the mixed layer are typically several weeks, a year, and a decade, respectively (Broecker and Peng 1982). Consequently, the Stommel demon should directly influence the transfer of oxygen and, to a lesser extent, that of carbon dioxide (Follows et al. 1995), but is not likely to be relevant for radiocarbon.

While this study has focused on the North Atlantic, the Stommel demon mechanism is likely to operate over other ocean basins. In each case, the main thermocline will acquire the water mass properties of the mixed layer at the end of winter, although this will appear as "March" waters in the Northern Hemisphere and "September" waters in the Southern Hemisphere. Accordingly, climate models should resolve the seasonal cycle or apply end of winter boundary conditions, otherwise the modeled thermocline will acquire an incorrect water mass structure.

Acknowledgments. RGW was supported in part under the NOAA Program in Climate and Global Change

and the NERC UK WOCE Special Topic Grant GST/02/813, MS by NOAA Grant NA90AA-D-AC498 under the Atlantic Climate Change Program and ONR Grant N00014-90-J-1490, and JCM in part by the National Science Foundation. We are grateful to Frank Bryan and Bill Holland for making available the CME model fields and would like to thank Mick Follows, David Marshall, and Tom Yates for useful discussions and computing assistance.

APPENDIX A

Tracer-Derived Subduction Relation

Consider the age distribution along a vertical section in Fig. A1 showing a mixed layer overlying a stratified thermocline—the section is aligned with the background horizontal flow. For simplicity, assume that the baroclinic shear is relatively small and that streamlines connect fluid subducted at f_0 with downstream observations where the Coriolis parameter is f.

The vertical spacing Δz_0 between a particle subducted along ρ_1 and the overlying mixed layer is given by the product of the instantaneous subduction rate S and the elapsed time, t, since the particle was in the mixed layer. Assuming that the age exactly measures the elapsed time t, then the subduction is given by

$$S_{\mathcal{J}} = \frac{\Delta z_0}{\mathcal{J}(\rho_1, f_0)}. \tag{A1}$$

Assuming that baroclinic shear and diffusion are not significant, then the age along streamlines on ρ_1 and ρ_2 should linearly increase with time between the boundary values at f_0 and the downstream observations at f:

$$\mathcal{J}(\rho_1, f) = \mathcal{J}(\rho_2, f) + \mathcal{J}(\rho_1, f_0). \tag{A2}$$

Assuming that the large-scale potential vorticity is conserved along the streamlines, then the vertical spacing at f_0 and f are related by

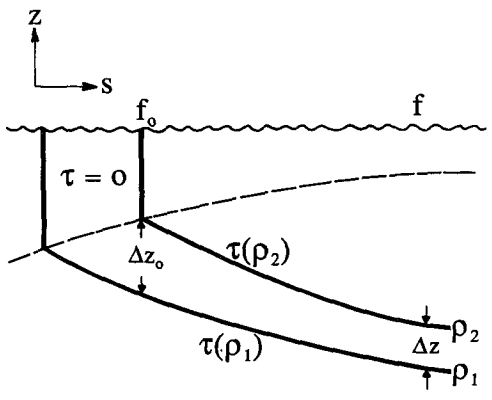

FIG. A1. A schematic diagram of a mixed layer and a stratified thermocline, which shows the age distribution, $\mathcal{J}$, and thickness, Δz, between isopycnals in the thermocline; the vertical section is aligned with the background flow.

$$\Delta z_0 = \frac{f_0}{f}\Delta z. \tag{A3}$$

Combining (A1) to (A3) gives the Jenkins (1987) relation between the subduction rate and the vertical gradient in the age field at a downstream location where the Coriolis parameter is f:

$$S_{\mathcal{J}} = \frac{f_0}{f}\left(\frac{\partial \mathcal{J}}{\partial z}\right)^{-1}.$$

The accuracy of the subduction relation is likely to decrease in time as diffusion and baroclinic shear distort the age field, preventing the age field from being unambiguously connected to the upstream values.

APPENDIX B

Tracer Integration

The date tracer field A, discussed in sections 4 and 5, identifies when fluid leaves the mixed layer and enters the thermocline. The water column is separated into a mixed layer overlying a stratified interior:

(i) Within the mixed layer, the tracer A is always set to have the same value as the time of year: 0 indicates the start of January and 1 the end of December for every year.

(ii) In the stratified interior, the tracer field A is initially set to -0.05 and, subsequently, A is found by solving the advection and diffusion equation:

$$\frac{\partial A}{\partial t} + \nabla\cdot(\mathbf{u}A) - \nabla(k\nabla A) = 0.$$

The tracer spreads into the interior through advection and diffusion from the source in the mixed layer.

The tracer integration uses 3 or 6 day fields of velocity $\mathbf{u}$, temperature T, and salinity S from annual cycles derived from the 1° or 1/3° CME integrations. The mixed layer thickness h is diagnosed over the year from the density field, which is calculated from the T and S fields; h is defined by the depth at which the density increases by 0.125 kg m^{-3} from the surface.

The tracer equation is integrated with an Euler-forward scheme using an "upwind" scheme, which is stable using a time step of 1/3 of a day to satisfy the CFL condition. The advective and diffusive fluxes are both set to zero on the coastal boundaries. At every grid point, the advective flux of the tracer, $\mathbf{u}A$, is found through each face of a cube surrounding a mass point using upwind differencing. The divergence of the advective flux, $\nabla\cdot(\mathbf{u}A)$, is then found with volume fluxes evaluated as in the CME to ensure conservation of volume.

The explicit diffusivity, k, is chosen to have a zero vertical value and a horizontal value of 10 m^2 s^{-1}. However, there is a larger implicit diffusion from the

upwind scheme that smears the tracer along streamlines with a magnitude of $\frac{1}{2}U\Delta x$, which for a flow of $U \sim 1$ cm s^{-1} and a grid spacing of $\Delta x \sim 30$ or 100 km gives an implicit diffusion of 150 or 500 m^2 s^{-1} along streamlines.

REFERENCES

Bleck, R., H. P. Hanson, D. Hu, and E. B. Kraus, 1989: Mixed layer–thermocline interaction in a three-dimensional isopycnic coordinate model. *J. Phys. Oceanogr.*, **19,** 1417–1439.

Broecker, W. S., and T.-H. Peng, 1982: *Tracers in the Sea.* Eldigio Press, 691 pp.

Bryan, F. O., and W. R. Holland, 1989: A high resolution simulation of the wind- and thermohaline-driven circulation of the North Atlantic Ocean. *Parameterizations of Small Scale Processes', 96–116. Proceedings 'Aha Huliko'a 89,* P. Muller and D. Henderson, Eds., Hawaii Inst. of Geophysics, Univ. of Hawaii, 382 pp.

Bryan, K., 1969: A numerical method for the study of the circulation of the World Ocean. *J. Comput. Phys.*, **4,** 347–376.

Camp, N. T., and R. L. Elsberry, 1978: Oceanic thermal response to strong atmospheric forcing II. The role of one-dimensional processes. *J. Phys. Oceanogr.*, **8,** 215–224.

Cox, M. D., 1984: A primitive equation, 3-dimensional model of the ocean. Ocean Group, Geophysical Fluid Dynamics Laboratory, Tech. Rep. 1, Princeton, NJ, 141 pp.

——, 1985: An eddy-resolving numerical model of the ventilated thermocline. *J. Phys. Oceanogr.*, **15,** 1312–1324.

Cushman-Roisin, B., 1987: *Dynamics of the Oceanic Surface Mixed-Layer.* P. Muller and D. Henderson, Eds., Hawaii Institute of Geophysical Special Publications, 181–196.

Federiuk, J. M., and J. F. Price, 1985: Mechanisms of oceanic subduction. Unpublished manuscript.

Follows, M. J., and J. C. Marshall, 1994: Eddy driven exchange at ocean fronts. *Ocean Modelling,* **102,** 5–9.

——, R. G. Williams, and J. C. Marshall, 1995: Subduction of carbon in the subtropical gyre of the North Atlantic. *J. Mar. Res.*, submitted.

Hellerman, S., and M. Rosenstein, 1983: Normal monthly wind stress over the World Ocean with error estimates. *J. Phys. Oceanogr.*, **13,** 1093–1104.

Huang, R. X., 1990: On the three-dimensional structure of the wind-driven circulation in the North Atlantic. *Dyn. Atmos. Oceans,* **15,** 117–159.

Iselin, C. O'D., 1939: The influence of vertical and lateral turbulence on the characteristics of waters at mid-depths. *Trans. Amer. Geophys. Union,* **20,** 414–417.

Jenkins, W. J., 1987: ^{3}H and ^{3}He in the beta triangle: Observations of gyre ventilation and oxygen utilization rates. *J. Phys. Oceanogr.*, **17,** 763–783.

——, 1988: The use of anthropogenic tritium and helium-3 to study subtropical gyre ventilation and circulation. *Philos. Trans. Roy. Soc. London, Ser. A,* **325,** 43–61.

Levitus, S., 1982: *Climatological Atlas of the World Ocean.* NOAA Prof. Paper 13, U.S. Govt. Printing Office, 173 pp.

Liu, Z., and J. Pedlosky, 1994: Thermocline forced by annual and decadal surface temperature variation. *J. Phys. Oceanogr.*, **24,** 587–608.

Luyten, J. R., J. Pedlosky, and H. Stommel, 1983: The ventilated thermocline. *J. Phys. Oceanogr.*, **13,** 292–309.

Marshall, D., and J. C. Marshall, 1995: On the thermodynamics of subduction. *J. Phys. Oceanogr.*, **25,** 138–151.

Marshall, J. C., and A. J. G. Nurser, 1991: A continuously stratified thermocline model incorporating a mixed layer of variable depth and density. *J. Phys. Oceanogr.*, **21,** 1780–1792.

——, ——, and R. G. Williams, 1993: Inferring the subduction rate and period over the North Atlantic. *J. Phys. Oceanogr.*, **23,** 1315–1329.

New, A. L., R. Bleck, Y. Jia, R. Marsh, M. Huddleston, and S. Barnard, 1995: An isopycnal model study of the North Atlantic. Part I: Model experiment. *J. Phys. Oceanogr.*, **25,** 2667–2699.

Pedlosky, J., and P. Robbins, 1991: The role of finite mixed-layer thickness in the structure of the ventilated thermocline. *J. Phys. Oceanogr.*, **21,** 1018–1031.

Pollard, R. T., and L. A. Regier, 1992: Vorticity and vertical circulation at an ocean front. *J. Phys. Oceanogr.*, **22,** 609–625.

Rhines, P. B., and W. R. Young, 1982: A theory of wind-driven circulation. I. Mid-ocean gyres. *J. Mar. Res.*, **40**(Suppl.), 559–595.

Spall, M. A., 1995: Frontogenesis, subduction and cross-front exchange at upper ocean fronts. *J. Geophys. Res.*, **100,** 2543–2557.

Stommel, H., 1979: Determination of watermass properties of water pumped down from the Ekman layer to the geostrophic flow below. *Proc. Natl. Acad. Sci. U.S.*, **76,** 3051–3055.

Williams, R. G., 1989: The influence of air–sea interaction on the ventilated thermocline. *J. Phys. Oceanogr.*, **19,** 1255–1267.

——, 1991: The role of the mixed layer in setting the potential vorticity of the main thermocline. *J. Phys. Oceanogr.*, **21,** 1803–1814.

Woods, J. D., 1985: Physics of thermocline ventilation. *Coupled Atmosphere–Ocean Models.* J. C. J. Nihoul, Ed., Elsevier, 543–590.